Cryomilling: An environment friendly approach of preparation large quantity ultra refined pure aluminum nanoparticles

Nirmal Kumar,[a] and Krishanu Biswas[a*]

Department of Material Science & Engineering, Indian Institute of Technology Kanpur, Kanpur India-208016

Abstract

The preparation of nanoparticles in large quantity is the challenge by most of the synthesis processes being used. Therefore, a present article reports a top down approach to synthesise large quantity aluminium nanoparticles (Al NPs). The cryomilling is known to be for ultra refinement particles size and suppress the rate of oxidation during synthesis. Aluminum metal is reactive metal and highly prone to oxidize/nitride in nanoscale. Therefore, a novel cryomill has been used to prepare large quantity Al NPs in which, the Al powder has been milled <123 K temperature. This technique does not leave any hazardous by-product and know to be environment friendly technique. The ultra refined Al NPs is a promising candidate for application in fields such as- explosive formulation, nanofluids, pigments, heat shield coating of aircrafts etc. Cryomilling approach, bulk synthesis of Al NPs will satisfy the increasing demand of Al NPs on an industrial scale. Therefore, this article addresses the Al NPs ultra refined phenomenon at cryo temperature. The prepared nanoparticles has been characterized in order to shape, size, dispersion stability, and purity of the Al NPs. Additionally, the thermal stability of nanoparticles, theoretically minimum grain size achievable at cryo temperature, and minimum sintering temperature of particles during milling has been discussed.

Keywords : Al nanoparticles, Cryomilling, Stability, High purity, Metal

#Corresponding author, e -mail- kbiswas@iitk.ac.in , Phone :+91-512-2596184, FAX:+91-512-2597505

1 Introduction

The pure metal nanoparticles have attracted attention to the researchers in the last few decade due to their high dispersity in the polar solvents, making them potential candidates for a variety of applications, including flexible printed large-area electronic[1], nanofluids [2], surface enhanced raman scattering photonic devices [3, 4]. These applications demand large scale production of pure free standing metallic nanoparticles with narrow size distribution. Most of the synthesis routes, utilized to prepare free standing metallic nanoparticles, stabilize the nanostructure by using capping agents [3, 5] to obtain narrow size distribution. However, the presence of a layer of the capping agent on the nanoparticles is detrimental for the desired properties in many applications. It is to be noted that the "free standing" nanoparticles are free from agglomeration without any surfactant or capping agents [6]. Ball milling at cryogenic temperatures (below 123K (-150 ^{o}C)) has been reported to be an effective method to prepare pure free standing nanoparticles in large quantity without the usage of any capping agent [7]. Recently, the preparation of various free standing metallic nanoparticles (Fe, Cu, Zn, Ag) using this method has been reported in the literature [6-10]. However, free standing aluminium nanoparticles, due to their rapid propensity to oxidization and nitridation has not been reported earlier. It is to be noted that there is substantial discussion in literature over efficacy of cryomilling process on increasing/decreasing of particles size. Earlier investigators have utilized attritor mills and wet milling (slurry of metallic powder with liquid nitrogen) to prepare metallic

nanoparticles. Zheng *et. al* [11] have reported that it is possible to reduce the particle size of Mg alloy (AZ80) from 55 μm to 10-30 μm after 8 hour cryomilling while average grain size is reported to 40 nm. In another study, particles size (55 μm) of Ti alloy is reported to increase to 120 μm in 2 hours cryomilling and later decrease to 44 μm particles size with 20 nm grain size during 8 hours cryomilling [12]. In another study reported average particles size of 99.9 wt % aluminium cryomilled with process agent (0.2% stearic acid) of 75 μm [13]. In the literature, the researchers predominantly utilized attritor mill for milling of powder with LN_2 (slurry form). Aluminium nanoparticles can also find various applications due to interesting physical, high enthalpy of combustion [14], enhance mechanical and electrical performance of epoxy based nanocomposite [15]. It is to be noted that aluminium powder is common ingredients for explosive formulation and it can ignite faster as the particle size gets smaller [16]. It has been reported that the addition of the nanoparticles in kerosene provides multiple heterogeneous nucleation sites to promote micro-explosions due to enhanced the evaporation rates of kerosene droplets at all tested temperature (673K (400 ^{o}C) – 1073K (800 ^{o}C)) [17]. In addition, high pure free standing aluminium nanoparticles can find application in aluminium pigments as well as heat shielding coating of aircraft [18-20].

A comprehensive literature survey indicates that the aluminium nanoparticles have been synthesized by many other processes including electrical discharge [21], wire explosion process [22], wet chemical synthesis [23, 24] arc plasma spray [25], aerosol synthesis [26], laser ablation [27] etc. In fact, a process called cryomelting; where spontaneous aluminium metal vapour condensed within a cryogenic medium has also been reported for preparation of aluminium nanoparticles. In this process, 60% of the particles is found to have size less than 70 nm with 3 nm alumina layer [28]. Similarly, another study using cryomelting has reported the preparation of aluminium particles having average grain size of 37 nm [29]. It has also been reported that the commercial pure aluminium particles consisting 1 wt% diamantane having average grain size of 22 nm exhibit greater thermal stability than pure Al nanoparticles in the temperature range of 423 (150 ^{o}C) to 773 (500 ^{o}C) K [30]. Some research groups have reported cryomilling of different types of aluminium alloys followed by consolidation [31, 32]. However, none of the studies reports the formation of pure free standing aluminium nanoparticles. In addition, the yield and purity of the nanoparticles are still

a challenge while the degree of agglomeration of the nanoparticles depends on the synthesis route. None of the above-mentioned techniques has reported successful synthesis of pure and free standing aluminium nanoparticles. On the other hand, the cryomilling involving mechanical grain refinement is expected to impart less contamination from the milling tools due to faster refinement at cryogenic temperature (<123K (-150 ^{o}C)) as well as protection from oxidation and nitridation compared to the room temperature ball milling. The oxide layer formation over particles surface can either be inhibited or substantially reduced due to extremely low temperature and inert gas environment during milling, resulting in the formation of nanoparticles with virgin surfaces, which can easily disperse in the polar solvents. In addition, any applications involving usage of high temperature (>100 ^{o}C) require the nanoparticles to be stable and therefore, it is important to investigate the stability of the as processed nanoparticles.

In the present investigation, we report a detailed study on the synthesis as well as the dispersion stability of the aluminium nanoparticles using cryomilling. This systematic study will discuss the successful synthesis of aluminium nanoparticles and thermal stability of the free standing nanoparticles. The results will be discussed using the model by Mohamad dealing with early grain refinement and ultrafine refinement during cryomilling [33]. The sintering model by Alymov *et al*. [34] has been utilized to discuss the ball milling conditions required to be satisfied for the formation of free standing nanoparticles.

2 Experimental details

2.1 Synthesis

The nanoparticles were prepared by cryomilling of aluminium powder 99.9 % purity (Alpha Aesar, USA; -40+325 mesh). The custom built cryomill using single tungsten carbide (WC) ball has been utilized in which, cryo temperature (<123 K) was maintained using liquid nitrogen (LN_2) in surrounding the milling chamber [35]. The powder was milled in dry, i.e., the powder and LN_2 did not come in contact during milling. The amplitude of the vibration in cryomilling was maintained 1.5 mm throughout the milling. The details of cryomill and working principle has been reported elsewhere [35]. The milling has been carried out under inert gas atmosphere

by purging Ar gas (1 litre/h) inside the milling vial. The real time temperature of the powder was monitored using a K-type thermocouple. A ball to powder ratio of 80:1 was utilised for the milling. The milling carried out for 6 hours and 30 minutes and the powder was intermittently collected each 30-minute interval for structural as well as microstructural analysis. The milled powder was dispersed in high purity (better than 99.9% purity) methanol to check the free standing ability. Sufficient care was taken to avoid any foreign contamination during handling of the milled powder.

2.2 Characterization

The X-ray diffraction patterns of synthesized powders were obtained using X-ray diffractometer (Bruker D8 Focus) with CuKα radiation (λ= 0.154056 nm) with step size 0.02°. The crystallite sizes and micro strain were estimated from peak broadening using Hall-Williamson approach [36]. The fine scale microstructure of the free - standing nanoparticles was obtained using transmission electron microscope (FEI, Tecnai G^2 UT 20 operated at 200 kV). A small amount of milled powder was dispersed in methanol and a few drops were placed on 400- mesh carbon coated copper TEM grid and dried in vacuum prior TEM analysis. In order to estimate foreign contamination due to handling of powder, nitridation, and oxidation of Al nanoparticles during ball milling, the milled powders were characterized using electron probe micro-analyzer (EPMA, JXA-8230, JEOL, Tokyo, Japan) as well as inductively coupled plasma mass spectrometry (ICP-MS, Thermo Scientific XSERIES 2 ICP-MS). The surface composition (few atomic layers) was estimated using X-ray photoelectron spectroscopy (XPS, PHI 5000 Versa Prob II, FEI Inc.) The cryomilled powder was annealed at different temperatures (323K (50 °C), 373K (100 °C), 423K (150 °C), and 473K (200 °C)) to study the thermal stability. The powder was kept in a vacuum sealed (10^{-6} bar) quartz tube prior to the heat treatment at any specified temperature for 2 hours.

3 Results

3.1 X-ray diffraction (XRD)

The Al powder (particle size ~ 10 μm) was cryomilled for up to 390 minutes and the samples were collected at 30 minutes interval for X-ray diffraction analysis. The XRD patterns of cryomilled powder are shown in Figure 1a. All the peaks in the patterns can consistently be indexed using reflections due to FCC aluminium (lattice parameter, a = 0.40494 nm: JCPDF No. 00-004-0787). No peak due to oxide or nitride could be detected to the best of the resolution of the XRD. The XRD pattern of the as-received powder is also shown at the bottom of Figure 1a for reference. It is evident that the diffraction peaks of the cryomilled powder show peak broadening (Figure 1a inset). In the process of cryomilling of powder, peak broadening can be due to nano-sized particle as well as micro-strain induced and therefore, one needs to carefully deconvolute the broadening due to particle size as well as micro- strain. The crystallite size and RMS (root mean square) micro-strain of the cryomilled powder have been estimated from the peak broadening using Hall –Williamson approach after substracting broadening due to the XRD machine. Figure 1b shows the variation of the crystallite size and the strain as a function of the time of milling.

The particle size decreases monotonically as a function of milling time. This is expected because of the fact the cryomilling leads to nanocrystal formation fast. The crystallite size of the cyomilled powder is observed to vary from 10 to 15 nm after 390 minutes of ball milling. The micro-strain initially increases reaching maximum value (0.21) at 210 min after cryomilling as shown in Figure 1b and then decreases to 0.17 at 390 minutes. This behaviour is due to change in the deformation mechanism of plastic deformation as the particle size decreases during cryomilling. It is to be noted that this strain is due to plastic deformation occurring within aluminium grains via generation and movement of dislocations. The increase of micro-strain in the particle is mainly due to dislocation- dominated deformation occurring in bigger particles (>100 nm), leading to the formation of small angle boundaries. As shown in Figure 1b, after 210 minutes of milling, crystallite size reaches in nanometric range (<100 nm). Nano-sized particles attribute to the energy release accompanying the fracture of the crystals after reaching a critical value of strain [37, 38]. In addition, we need to consider stacking fault in FCC aluminium. The stacking faults in nano grain size will be eliminated due

to the instability of partial Shockley dislocations when grain size becomes comparable with the equilibrium distance between two partial dislocations [39].

3.2 Dispersion stability (free standing behaviour)

In order to check free standing or dispersion stability (without surfactant), the cryomilled powder was dispersed in ultra pure methanol, following ultrasonication for 10 minutes. Figure 2 shows the results of the investigation on the powder milled for 390 minutes. Figure 2a is the optical image of the test tube containing Al NPs dispersed in methanol. For clarity, the optical image of a test tube containing only methanol is also shown in both Figures 2a and 2b. The good dispersion of Al NPs is visible in the image. In fact, the inverted image (inverse contrast) is also shown for betterment of the contrast. The nanoparticles are observed to be stable in methanol after 10 days (as shown in Figure 2b). In fact, the nanoparticles have been found to remain well dispersed in methanol even after 2 months. Thus, it is evident that the Al nanoparticles are highly stable in methanol and there is no tendency to fast agglomeration. Similar experiments carried out using other polar solvents, such as ethanol, ethylene glycol etc; indicate the similar behaviour of the nanoparticles.

3.3 Transmission electron microscopic (TEM) observation

To obtain finer scale micro structural information (size, shape, distribution, and defect structure etc), the milled powder was investigated using TEM. The cryomilled powder dispersed in methanol was taken out from the test tubes with the help of micropipette and dropped on carbon coated 400-mesh Cu grid. The grid was subsequently dried in vacuum over night prior to TEM observation. The Figure 3a shows a typical bright field micrograph showing Al NPs, free from agglomeration with nearly spherical geometry. Figure 3b shows the corresponding histogram, indicating narrow distribution of nanoparticles (7±3 nm) after cryomilling. The histogram was obtained using a large number of high resolution bright field TEM micrographs. Figure 3d shows a high resolution image of one such nano-particle with inset showing FFT (Fast Fourier Transform) of the selected region (marked on the Figure).

It shows large number of dislocation accumulation in nanoparticles during cryomilling. The SAED pattern (Figure 3c) indicates the spotty diffraction rings due to aluminium only, indicating the presence of pure aluminium nanoparticles.

3.4 Purity of nanoparticles

It has already been reported that the cryomilling can be used for the preparation of high purity metal nanoparticles for a variety of applications [35]. A comprehensive compositional measurements of the milled powder have been carried out to confirm the purity of the nanoparticles. The composition of cryomilled powder analyzed using electron probe micro analyzer (EPMA) as well as inductively coupled plasma mass spectroscopic (ICP-MS) technique. Figure 4 shows the results obtained using EPMA investigation on Al powder cryomilled for 390 minutes. The presence of carbon peak, arising from the carbon tape used for mounting the powder sample is observed. Thus, no other impurity has been detected within the detection limit of EPMA (100 ppm). Further, the milled powder was investigated using ICP-MS, which is sensitive to presence of the trace elements (detection limit of 1 ppb). The detailed ICP-MS investigation shows the presence of W (3 ppm) in the milled powder. The impurities from milling tool (W from ball and vial) cannot be avoided. This is negligible amount compared to room temperature ball milling [40].

3.5 X-ray photoelectron spectroscopy

The surface oxygen has been estimated using XPS and compared with as received Al powder. It is to be noted that the process has not used any hazardous chemical during the preparation of nanoparticles and thus, it can be considered a green synthesis process [41] for the preparation of high purity aluminium nanoparticles. In this process the particles have not been capped with any surfactant. Therefore, XPS has been utilized, which is highly sensitive to surface analysis, ideal for few outermost atomic layer [42] and the all peaks has been referenced (charge correction) with adventitious carbon 284.8 eV. Therefore, the Figure 5 (a-b) shows that oxide layer present over surface of the as received Al powder particles. The total O concentration is contributed by adsorbed contamination (533.5 eV) [43], aluminum in hydroxide/oxyhydroxide (532.4 eV) [44, 45] and aluminum oxide layer (531.33 eV) [46]. In fact, a careful analysis reveals that the oxygen contribution from oxide is 9 atom % out of total oxygen concentration. Further comparing with cryomilled powder, Figure 5 (c-d) shows that over all Al metal concentration is slightly increased and oxygen concentration (quantification shown in Table 1) remains almost unchanged during cryomilling. Thereafter, O 1s peak of cryomilled powder was further deconvoluted and

shown in Figure 5 (e). It indicates that the oxygen contribution from the oxide layer is about 21.5 atom % out of total O concentration. Therefore, the oxide layer contributed O concentration has increased 12.5 atom % after cryomilling. The increased oxide is mainly due to large number of nanoparticles (large surfaces area), which consist thin layer of oxide. The cryomilled powder does not have any other impurities. C is inadvertently present as shown [Figure 5 (f)] in survey spectra of cryomilled Al powder. The sample has been exposed in environment during sampling in XPS for a short time which is might be reason for C and thin layer formation of oxide over nanoparticles. In addition, the nanoparticles surfaces highly prone to formed oxide (reduce to energy with binding oxygen and organic contamination). Thus, it can be concluded that the oxide thin layer always present over the aluminium nanoparticles surfaces. The cryomilling has not introduced extra contamination and this technique has capability to protect powders from further oxidation.

3.6 Thermal stability

As the metal nanoparticles are highly prone to agglomerates and grain growth due to the large surface area to volume ratio, it is worthwhile to study the thermal stability of the cryomilled nanoparticles. In addition, many potential applications require the usage of the aluminium nanoparticles at elevated temperature (>373K (100 ^{o}C)) and the thermal stability of the nanoparticles plays a critical role in deciding the usage. Thus, annealing or heat treatment at different temperatures (323K (50 ^{o}C), 373K (100 ^{o}C), 423K (150 ^{o}C), and 473 K (200 ^{o}C)) for 2 hours in inert atmosphere has been used to systematically study the thermal stability of the cryomilled aluminium nanoparticles. The annealing temperatures have been selected in such a way that it varies from 0.075 – 0.3 T_m, where T_m is the melting temperature of pure aluminium. It is expected that nanocrystalline grains of the cryomilled powder will exhibit growth during the heat treatment. Subsequently, the microstructural investigation of the annealed powder has been carried out using TEM. Figures 6(a-d) show the bright field TEM micrographs whereas Figures 6(a'-d') illustrate the histograms showing the particle size or grain size distribution. Figure 5b inset shows the SAED pattern from a nanoparticle, which is evidence of FCC aluminium. One can clearly observe the coarsening of particles with increasing heat treatment temperature. Initially, the nanoparticles with narrow size distribution (Fig 3b) undergo coarsening with wide size

distribution, indicating anomalous growth. The detailed particle size analysis indicates that the nanoparticles do not grow much until 373 K (100 ^{o}C). However, annealing at 423 K (150 ^{o}C) and 473 K (200 ^{o}C) leads to the formation of particles having sizes more than 100 nm. The annealing at 473 K (200 ^{o}C) shows a bimodal distribution of particles with some particles even growing up to 200 nm. The anomalous coarsening behaviour of nano-crystalline aluminum particles is responsible for the bimodal distribution of the particles.

The some nanoparticles coarsen rapidly to due favourable surface energy. The temperature of 200 °C has been found to be enough for the nanoparticles to grow fast while particles are in contact. Some other particles do grow relatively slowly and thus, it leads to bimodal distribution of particles. Figure 6e shows the coarsening behaviour of the nanoparticles as a function of annealing temperature. Another important observation of the annealing treatment is the change of shape of the nanoparticles. The as prepared nanoparticles having near spherical shape undergo shape change to cuboidal shape at a higher temperature (373 K (100 ^{o}C), 423 K (150 ^{o}C) and 473 K (200 ^{o}C)). The higher magnification micrographs as shown in the inset of Figures 6(a-d) reveal the shape of the particles. Initially particles remain in spherical shape and then achieve cuboidal shape at higher temperature. This is because of the fact that post necking, the particles rotate to minimize grain boundary energy (inset Figure 6d). It is to be noted that these images have been obtained when the nanoparticles are oriented along <001> direction. This aspect is under investigation and will be communicated separately.

3.7 Discussion

The present investigation, for the first time, shows the successful synthesis of high pure Al NPs using ball milling at cryogenic temperature. The Al NPs nanoparticles have been found to be of high purity, devoid of oxides or nitrides. The only impurity in minute quantity observed in the cryomilled nanoparticles is tungsten, originating from the milling media. The nanoparticles have also been found to be stable (retainment of size in the nanometric domain) during annealing treatment up to 373 K (100 ^{o}C).

These novel experimental findings need explanation. In the following, we shall discuss the results in the light of available literature. Free standing or isolated nanoparticles have been studied extensively in past decades in order to extract their intrinsic

properties, which are useful for device applications and thus, these are of foremost importance to the scientific and technological communities. The bulk preparation of Al NPs is scarcely reported in the literature [6, 7, 10, 35, 9]. It is expected that ball milling at cryogenic temperature can be used for the synthesis of different metallic nanoparticles in large quantity. Therefore, it is imperative to understand the synthesis of the free standing nanoparticles of controlled particle size by ball milling at cryogenic temperature. Fundamentally, the preparation of free standing nanoparticles is decided by the competition between cold welding and fracturing during ball milling [6]. In the five stages of mechanical milling [47], fracture dominate over cold welding [40]. These two factors strongly depend on the milling temperature. Mechanical milling is a process in which powders are charged in the vial of the ball mill and then caused to be collided by moving balls. The process can be carried out using attritor, SPEX shaker mill, a planetary mill, horizontal ball mill etc. During high-energy milling, the powder particles are repeatedly flattened, cold-welded, fractured, and rewelded [48]. Since powders are cold welded and fractured during milling, it is critical to establish a balance between cold welding and fracturing during milling for the preparation of the free standing nanoparticles of narrow size distribution. The ability of cold welding and fracturing of powder depends on the material and the milling conditions. Every metal requires some threshold deformation to start cold bonding. Soft materials, such as aluminium, normally have good weld ability at room temperature and the rise in temperature during milling (normally observed during conventional milling) helps to cold bond easily with low percent deformation. It is difficult to overcome the cold welding phenomena even during conventional milling. Therefore, the ultra refinement of particles is impossible by conventional ball milling. However, cooling of powders is considered as an effective approach to accelerate the fracture process as well as suppress the process of cold welding, recovery and recrystallization, leading to rapid grain refinement[49,50]. It is well known that fracturing of any material depends on temperature. A material, when cooled below ductile-to-brittle (DBT) temperature, will undergo brittle fracture and breaks very easily. Cooling down to very low temperature (123 K (-150 ^{o}C) to 96 K (-177 ^{o}C)) during cryo-milling is an effective means to accelerate this fracturing process for many materials having bcc and hcp crystal structure. However, materials having fcc crystal structure do not undergo any DBT transition in the specified temperature range [51].

Nonetheless, the fracturing tendency of the metals having fcc crystal structure will substantially increase at low temperature as compared to that at room temperature.

On the other hand, the cold welding can substantially be reduced at very low temperature. The ball milling of powder is thought to involve following processes; flattening of powder particles, welding of powder particles, formation of a layered structures, deformation of the layered structure and formation of nanoparticles. Therefore, it is clearly evident that the welding process due to collision of balls with powder during milling can be approximated as cold welding of two plates under pressure [52]. The increase in pressure during collision increases the real area of contact between the powders. According to cold–welding theory, the cold-welded bond of reasonable strength is associated with a particular range (40-70%) of deformation (plastic) strain of powders. The minimum deformation strain required for a cold welded bond depends on the materials systems employed and the temperature [52]. Most important aspect of cold welding is the fact that the bond strength between the powder particles of the metal is a function of deformation strain. For cold welding to occur, the deformation strain of the powder per collision event should be greater than the critical amount of deformation required to form a reasonably strong bonding. Thus, the strength of the weld depends on the ability of the material to undergo plastic deformation during milling. At extremely low temperatures (123 K (-150 ^{o}C) to 95 K (-177 ^{o}C)), the weld strength is expected to be poor for many of the useful metals because the minimum amount of deformation strain required to form a cold weld (40-70%) cannot be achieved [53, 54]. In case, the investigated metal does not undergo such an amount of deformation to form a cold welded joint during cryomilling, the fracturing process is expected to dominate during ball milling at low temperatures. It is also expected that even if some cold-welding takes place, then during subsequent collisions with balls, the cold-welded structure will break as the strength of the bonding will not be sufficient enough. Therefore, both will promote the formation of free standing nanoparticles. The cold welding can effectively be suppressed in cryomilling, which helps to achieve ultrafine particles size with early grain refinement. The formation of cold welded joint of sufficient strength, the minimum deformation required is 60%. For a metal like aluminium, 60% reduction during ball milling at cryogenic temperature is extremely difficult to achieve. Hosford *et al.* [55] have shown that aluminium failed at true tensile strain of 0.3 at 77 K temperature.

Therefore, it is difficult to form good cold welded joints at 77 K. Thus, fracturing of the aluminium particles will dominate over cold welding during ball milling at cryogenic temperatures (<123 K (-150 ^{o}C)) and this will lead to the formation of ultra refined Al NPs.

In addition, we also need to discuss the formation of AL NPs of narrow size range during the process of cryomilling. The present investigation shows that it is possible to form nanoparticles in the size range of 7±3 nm during cryomilling. Mohamed has provided a relationship between the minimum grain size achievable during ball milling with materials and processing parameters [33].

$$\frac{d_{\min}}{b} = A\left\{\left(\exp\left(\frac{-\beta Q}{RT}\right)\left(\frac{D_{PO}Gb^2}{\nu_o kT}\right)^{0.25} \times \left(\frac{\gamma}{Gb}\right)^{0.5}\left(\frac{G}{H}\right)^{1.25}\right)\right\} \quad (1)$$

,where b is Burger's vector of dislocation, A (dimensionless constant), β is a constant (0.04); Q the self-diffusion activation energy, Dpo pipe diffusion coefficient [56], ν_o passion's ratio, γ stacking fault energy, G shear modulus, H hardness, R the universal gas constant, k the Boltzmann constant and T is the absolute temperature. According to the equation, d_{min} is strongly dependent on the milling temperature because the values of Q, D_{P0}, G, H are dependent on T. In the present case, the milling temperature of the aluminium powder has been maintained below 123 K (-150 ^{o}C). Using the materials properties for aluminium (as listed in Table 2), one can obtain d_{min} to be 11 nm, which is reasonably close to the experimentally observed size range of the nanoparticles (7±3 nm), obtained after cryomilling for 330 minutes.

Although cryomilling involves low-temperature processing, the milling can lead to the generation of heat at the particle-particle interface locally and hence can increase the local temperature. In addition, the thermal component of the applied stress, as well as driving force due to the reduction of surface energy, can cause sintering of the freshly formed free standing nanoparticles. Therefore, the formation of free standing nanoparticles is possible during ball milling provided the thermal processes can be even avoided or suppressed. Thus, milling parameters must be selected in such a way that thermally controlled sintering of the free standing nanoparticles can be avoided. According to Alymov et al. [34] the sintering temperature (T_{SS}) of nano or ultrafine particles is given by

$$T_{SS} = T_m \ln\{1 + k(e-1)\} \quad (2)$$

, where,

$$k = \frac{A}{\left((L+1) - (L+1)^{\frac{2}{3}}\right)} \quad (3)$$

$$T_m = T_0\left(1 + \frac{(\gamma_l - \gamma_s)}{\Delta H_{m,o}} . \frac{3}{d}\right) \quad (4)$$

,where k is the fraction of sintered region, as defined in equation (3), A is a constant varying from 0.06 to 0.15; L the number of a neighbour of a particle and T_m is the melting temperature defined in equation 4 [57]. T_m is the bulk melting temperature, γ_l and γ_s are surface tension liquid and solid respectively, $\Delta H_{m,o}$ the melting enthalpy and d is the crystallite size. The values of the parameters utilized for calculation of T_{ss} are provided in Table 2. The calculations indicate that T_{ss} ~ 130 K (-143 ^{o}C) for d = 7 nm. Thus, the milling parameters must be selected in such a way that T_{ss} is not reached. It is now important to estimate the rise in temperature during the process of cryomilling in the present investigation. According to Schwarz *et al*. [58], the rise in temperature due to localized shear of the powder particles entrapped between the ball and vial during milling is given by

$$\Delta T = \frac{F}{2} . \left(\frac{\Delta t}{\pi k \rho C_P}\right)^{1/2} \quad (5)$$

Here, ΔT is the rise in temperature, F dissipated energy flux = σ.V, where σ = normal stress caused by the head-on collision and V is the relative velocity of the balls before impact, Δt the stress state lifetime, ρ powder particle density, k thermal conductivity of powder and C_P is heat capacity of powder [listed in Table 3]. Here, σ can be approximated as the maximum compressive stress generated by a head-on collision of two balls of diameter D and thus, σ is given by

$$\sigma = 0.616\left[P.E^2\left(\frac{2}{D}\right)^2\right]^{1/3} \quad (6)$$

,where E is the elastic modulus of the ball, P load. Using the values of parameters listed in Table 3 the calculated value of ΔT = 4 K or 4 ^{o}C due to localized heating due

to impact between ball and vial. Therefore, the actual temperature of impacted powder (123±4 K) lies below the sintering start temperature (T_{SS} ~ 130 K (-143 ^{o}C)). Thus, milling condition has been performed in such a way that d_{min} and T_{SS} lies lowest plastic deformation dominated region as shown in Figure 7. Sintering of aluminium nanoparticles is not expected to occur during cryomilling and formation of ultra refined free standing nanoparticles is a distinctly possible under the experimental conditions used in the present investigation, which fall under plastic dominated regime shown in Figure 7 .

3.8 Conclusions

The process of cryomilling can effectively be utilized for preparation of high pure free standing aluminium nanoparticles. The following conclusions can be drawn.

i) The particles prepared by cryomilling free stand in pure methanol for longer duration without any surfactant or stabilizers.

ii) The cryomilling process is capable of preparing nanoparticles with narrow distribution range (7-10 nm) particles.

iii) Low temperature helps to reduce the cold metallurgical bonding between particles during milling. The formation of free nanoparticles is predominantly controlled by fracturing rather than cold welding.

iv) The aluminium nanoparticles are thermally stable up to 373 K (100 ^{o}C).

v) The experimental results indicate that the formation of free standing aluminium nanoparticles is due to experimental conditions, which suppress the dynamic recovery and sintering processes.

Acknowledgements

The authors would like to acknowledge financial support from the SERB-DST India.

References

1. Rajan K, Roppolo I, Chiappone A, Bocchini S, Perrone D, Chiolerio A. Silver nanoparticle ink technology: State of the art. Nanotechnol Sci Appl 2016; 9:1-13.

2. Devendiran DK, Amirtham VA. A review on preparation, characterization, properties and applications of nanofluids. Renew Sustainable Energy Rev 2016; 60:21-40.

3. Tao AR, Habas S, Yang P. Shape control of colloidal metal nanocrystals. Small 2008; 4 (3):310-325.

4. Hazra B, Das K, Das Chakraborty S, Verma MS, Devi MM, Katiyar NK, et al. Hollow Gold Nanoprism as Highly Efficient "Single" Nanotransducer for Surface-Enhanced Raman Scattering Applications. J Phys Chem C 2016; 120 (44):25548-25556.

5. Rao CNR, Ramakrishna Matte HSS, Voggu R, Govindaraj A. Recent progress in the synthesis of inorganic nanoparticles. Dalton Transactions 2012; 41 (17):5089-5120.

6. Barai K, Tiwary CS, Chattopadhyay PP, Chattopadhyay K. Synthesis of free standing nanocrystalline Cu by ball milling at cryogenic temperature. Mater Sci Eng A 2012; 558 (0):52-58.

7. Tiwary C, Verma A, Kashyp S, Biswas K, Chattopadhyay K. Preparation of Freestanding Zn Nanocrystallites by Combined Milling at Cryogenic and Room Temperatures. Metall Mater Trans A 2013; 44 (4):1917-1924.

8. Tiwary CS, Verma A, Biswas K, Mondal AK, Chattopadhyay K. Preparation of ultrafine CsCl crystallites by combined cryogenic and room temperature ball milling. Ceram Int 2011; 37 (8):3677-3686.

9. Verma A, Biswas K, Tiwary C, Mondal A, Chattopadhyay K. Combined Cryo and Room-Temperature Ball Milling to Produce Ultrafine Halide Crystallites. Metall Mater Trans A 2011; 42 (4):1127-1137.

10. Tiwary CS, Kashyap S, Biswas K, Chattopadhyay K. Synthesis of pure iron magnetic nanoparticles in large quantity. J Phys D: Appl Phys 2013; 46 (38):385001-385005.

11. Zheng B, Ertorer O, Li Y, Zhou Y, Mathaudhu SN, Tsao CYA, et al. High strength, nano-structured Mg–Al–Zn alloy. Mater Sci Eng A 2011; 528 (4–5):2180-2191.

12. Sun F, Rojas P, Zúñiga A, Lavernia EJ. Nanostructure in a Ti alloy processed using a cryomilling technique. Mater Sci Eng A 2006; 430 (1–2):90-97.
13. Liu D, Xiong Y, Li P, Lin Y, Chen F, Zhang L, et al. Microstructure and mechanical behavior of NS/UFG aluminum prepared by cryomilling and spark plasma sintering. J Alloys Compd 2016; 679:426-435.
14. Cooper PW. Explosives engineering. Wiley-VCH, 1996
15. Dong L, Zhou W, Sui X, Wang Z, Cai H, Wu P, Zhang Y, Zhou A. Mechanical and Electrical Properties of Aluminum/Epoxy Nanocomposites. J Electron Mater 2016; 45 (11):5885-5894.
16. Mench MM, Yeh CL, Kuo KK. Propellant burning rate enhancement and thermal behavior of ultra-fine aluminum powders (Alex). 29th Int Annual Conference of ICT 1998:30-31.
17. Javed I, Baek SW, Waheed K, Ali G, Cho SO. Evaporation characteristics of kerosene droplets with dilute concentrations of ligand-protected aluminum nanoparticles at elevated temperatures. Combust Flame 2013; 160 (12):2955-2963.
18. Ghorbani HR. A review of methods for synthesis of Al nanoparticles. Orient J Chem 2014; 30 (4):1941-1949.
19. Karlsson P, Palmqvist AEC, Holmberg K. Surface modification for aluminium pigment inhibition. Adv Colloid Interface Sci 2006; 128-130:121-134.
20. Moore AL, Shi L. Emerging challenges and materials for thermal management of electronics. Materials Today 2014; 17 (4):163-174.
21. Sahu RK, Hiremath SS, Manivannan PV, Singaperumal M. An Innovative Approach for Generation of Aluminium Nanoparticles Using Micro Electrical Discharge Machining. Procedia Materials Science 2014; 5:1205-1213.
22. Sarathi R, Sindhu TK, Chakravarthy SR. Generation of nano aluminium powder through wire explosion process and its characterization. Mater Charact 2007; 58 (2):148-155.
23. Haber JA, Buhro WE. Kinetic instability of nanocrystalline aluminum prepared by chemical synthesis; facile room-temperature grain growth. J Am Chem Soc 1998; 120 (42):10847-10855.
24. Lee HM, Kim YJ. Preparation of size-controlled fine Al particles for application to rear electrode of Si solar cells. Sol Energy Mater Sol Cells 2011; 95 (12):3352-3358.

25. Mandilas C, Daskalos E, Karagiannakis G, Konstandopoulos AG. Synthesis of aluminium nanoparticles by arc plasma spray under atmospheric pressure. Mater Sci Eng B 2013; 178 (1):22-30.
26. Kaplowitz DA, Jouet RJ, Zachariah MR. Aerosol synthesis and reactive behavior of faceted aluminum nanocrystals. J Cryst Growth 2010; 312 (24):3625-3630.
27. Gaertner GF, Lydtin H. Review of ultrafine particle generation by laser ablation from solid targets in gas flows. Nanostruct Mater 1994; 4 (5):559-568.
28. Champion Y, Bigot J. Synthesis and structural analysis of aluminum nanocrystalline powders. Nanostruct Mater 1998; 10 (7):1097-1110.
29. Molinari A, Demetrio K, Lonardelli I, Menapace C, Zadra M Spark plasma sintering of nanostructured aluminum powders produced by cryomilling. In: Advances in Powder Metallurgy and Particulate Materials - 2009, 2009. pp 972-978
30. Maung K, Mishra RK, Roy I, Lai LC, Mohamed FA, Earthman JC. Thermal stability of cryomilled nanocrystalline aluminum containing diamantane nanoparticles. J Mater Sci 2011; 46 (21):6932-6940.
31. Ye J, Ajdelsztajn L, Schoenung JM. Bulk nanocrystalline aluminum 5083 alloy fabricated by a novel technique: Cryomilling and spark plasma sintering. Metall Mater Trans A 2006; 37 (8):2569-2579.
32. Roy I, Chauhan M, Mohamed FA, Lavernia EJ. Thermal stability in bulk cryomilled ultrafine-grained 5083 Al alloy. Metall Mater Trans A 2006; 37 (3):721-730.
33. Mohamed FA. A dislocation model for the minimum grain size obtainable by milling. Acta Materialia 2003; 51 (14):4107-4119.
34. Alymov MI, Maltina EI, Stepanov YN. Model of initial stage of ultrafine metal powder sintering. Nanostruct Mater 1994; 4 (6):737-742.
35. Kumar N, Biswas K. Fabrication of novel cryomill for synthesis of high purity metallic nanoparticles. Rev Sci Instrum 2015; 86 (8):083903-083908.
36. Williamson GK, Hall WH. X-ray line broadening from filed aluminium and wolfram. Acta Metallurgica 1953; 1 (1):22-31.
37. Hellstern E, Fecht HJ, Fu Z, Johnson WL. Structural and thermodynamic properties of heavily mechanically deformed Ru and AlRu. J Appl Phys 1989; 65 (1):305-310.
38. Trudeau ML, Schulz R, Zaluski L, Hosatte S, Ryan DH, Doner CB, et al. Nanocrystalline Iron-Titanium Alloys Prepared by High-Energy Mechanical Deformation. Mater Sci Forum 1992; 88-90:537-544.

39. Oleszak D, Shingu PH. Nanocrystalline metals prepared by low energy ball milling. J Appl Phys 1996; 79 (6):2975-2980.
40. Han BQ, Ye J, Tang F, Schoenung J, Lavernia EJ. Processing and behavior of nanostructured metallic alloys and composites by cryomilling. J Mater Sci 2007; 42 (5):1660-1672.
41. Kumar N, Biswas K, Gupta RK. Green synthesis of Ag nanoparticles in large quantity by cryomilling. RSC Advances 2016; 6 (112):111380-111388.
42. Tougaard S. Energy loss in XPS: Fundamental processes and applications for quantification, non-destructive depth profiling and 3D imaging. J Electron Spectrosc Relat Phenom 2010; 178–179:128-153.
43. Bagus PS, Brundle CR, Illas F, Parmigiani F, Polzonetti G. Evidence for oxygen-island formation on Al(111): Cluster-model theory and x-ray photoelectron spectroscopy. Physical Review B 1991; 44 (16):9025-9034.
44. Cordier F, Ollivier E. X-ray photoelectron spectroscopy study of aluminium surfaces prepared by anodizing processes. Surf Interface Anal 1995; 23 (9):601-608.
45. Hess A, Kemnitz E, Lippitz A, Unger WES, Menz DH. ESCA, XRD, and IR Characterization of Aluminum Oxide, Hydroxyfluoride, and Fluoride Surfaces in Correlation with Their Catalytic Activity in Heterogeneous Halogen Exchange Reactions. J Catal 1994; 148 (1):270-280.
46. Kovacich JA, Lichtman D. A qualitative and quantitative study of the oxides of aluminum and silicon using AES and XPS. J Electron Spectrosc Relat Phenom 1985; 35 (1):7-18.
47. Benjamin JS, Volin TE. Mechanism of mechanical alloying. Metall Trans 1974; 5 (8):1929-1934.
48. Fecht HJ. Nanostructure formation by mechanical attrition. Nanostruct Mater 1995; 6 (1–4):33-42.
49. Suryanarayana C. Mechanical alloying and milling. Prog Mater Sci 2001; 46 (1–2):1-184.
50. Zhang Z, Han BQ, Zhou Y, Lavernia EJ. Elevated temperature mechanical behavior of bulk nanostructured Al 5083-Al85Ni10La5 composite. Materials Science and Engineering A 2008; 493 (1-2):221-225.
51. Dieter GE. Mechanical metallurgy. McGraw-Hill, 1986
52. Messler RW. Principles of Welding: Processes, Physics, Chemistry, and Metallurgy. Wiley, 2008

53. Vaidyanath LR, Nicholas MG, Milner DR. Pressure welding by rolling. Brit Weld J 1959; 6:1-13.
54. Alexander JM, Brewer RC (1963). In: London (ed) Manufacturing Properties of Materials. D. Van Nostrand, Boston, pp 363-369
55. Hosford Jr WF, Fleischer RL, Backofen WA. Tensile deformation of aluminum single crystals at low temperatures. Acta Metallurgica 1960; 8 (3):187-199.
56. Luthy H, Miller AK, Sherby OD. The stress and temperature dependence of steady-state flow at intermediate temperatures for pure polycrystalline aluminum. Acta Metallurgica 1980; 28 (2):169-178.
57. Guisbiers G, Pereira S. Theoretical investigation of size and shape effects on the melting temperature of ZnO nanostructures. Nanotechnology 2007; 18 (43):435710.
58. Schwarz RB, Koch CC. Formation of amorphous alloys by the mechanical alloying of crystalline powders of pure metals and powders of intermetallics. Appl Phys Lett 1986; 49 (3):146-148.

59. Brandes EA, Brook GB. General physical properties of light metal alloys and pure light metals. In: Brook EABB (ed) Smithells Light Metals Handbook. Butterworth-Heinemann, Oxford, pp 5-13. 1998

60. Bainbridge IF, Taylor JA. The surface tension of pure aluminum and aluminum alloys. Metall Mater Trans A 2013; 44 (8):3901-3909

61. Murr VLE. Interfacial Phenomena in Metal and Alloys Physik in unserer Zeit 1977; 8 (1):30-30

62. Desai PD. Thermodynamic properties of aluminum. Int J Thermophys 1987; 8 (5):621-638

Figures-

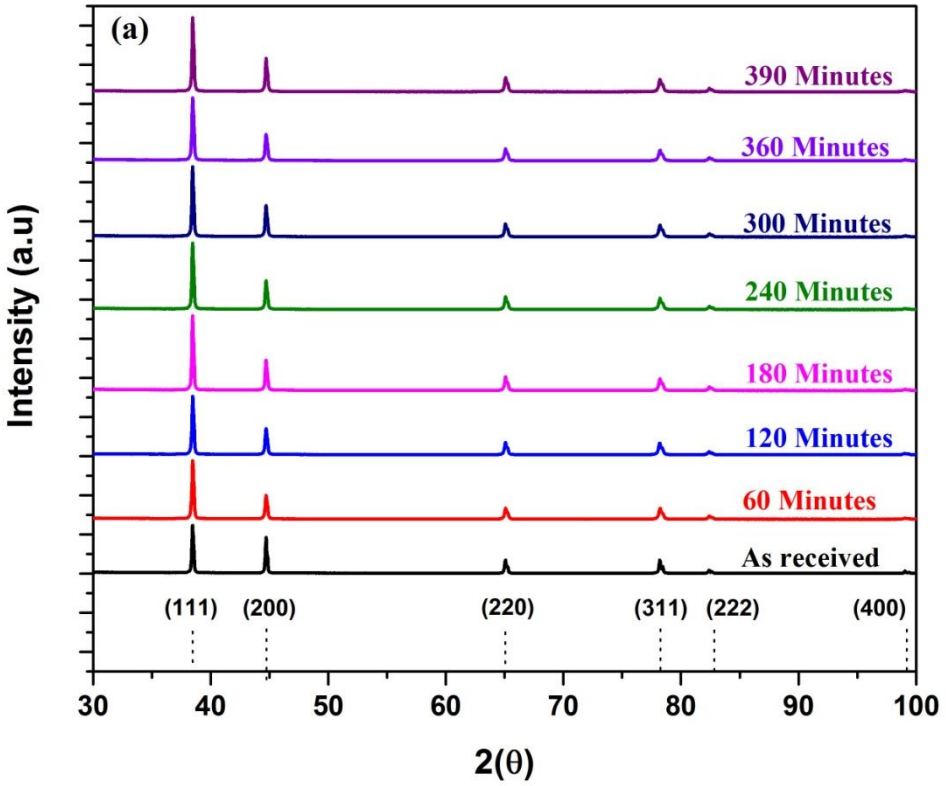
(a)
390 Minutes
360 Minutes
300 Minutes
240 Minutes
180 Minutes
120 Minutes
60 Minutes
As received
(111)
(200)
(220)
(311)
(222)
(400)
Intensity (a.u)
30
40
50
60
70
80
90
100
2(θ)

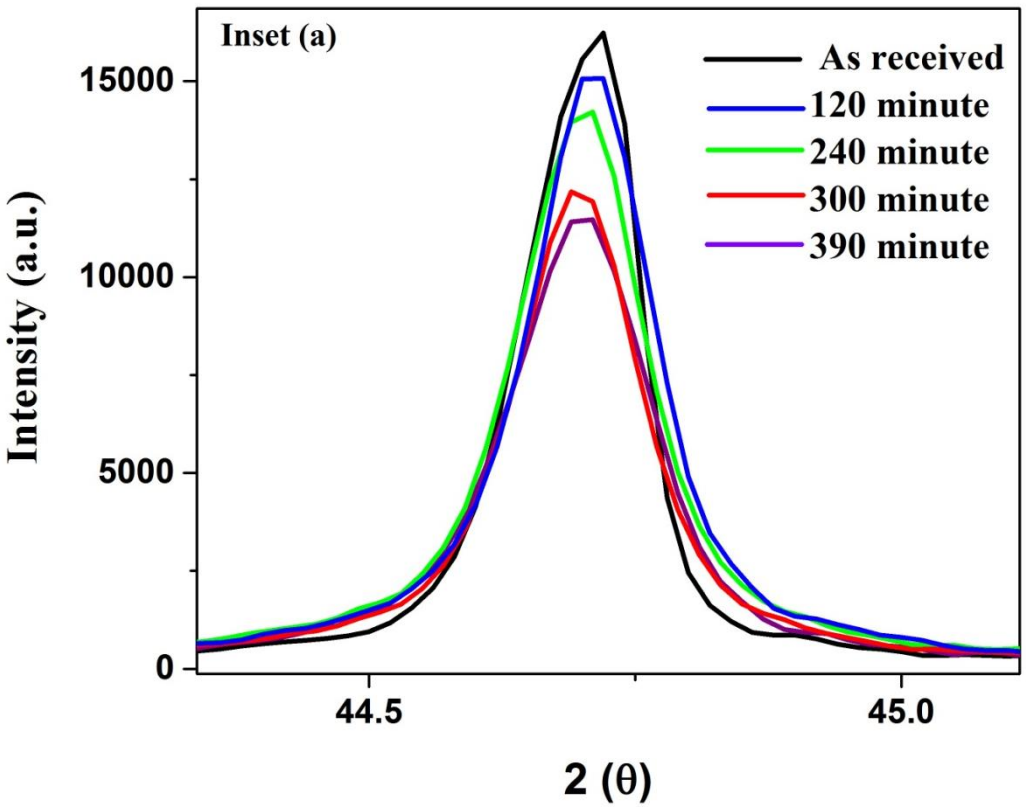
Inset (a)
As received
120 minute
240 minute
300 minute
390 minute
15000
10000
5000
0
Intensity (a.u.)
44.5
45.0
2 (θ)

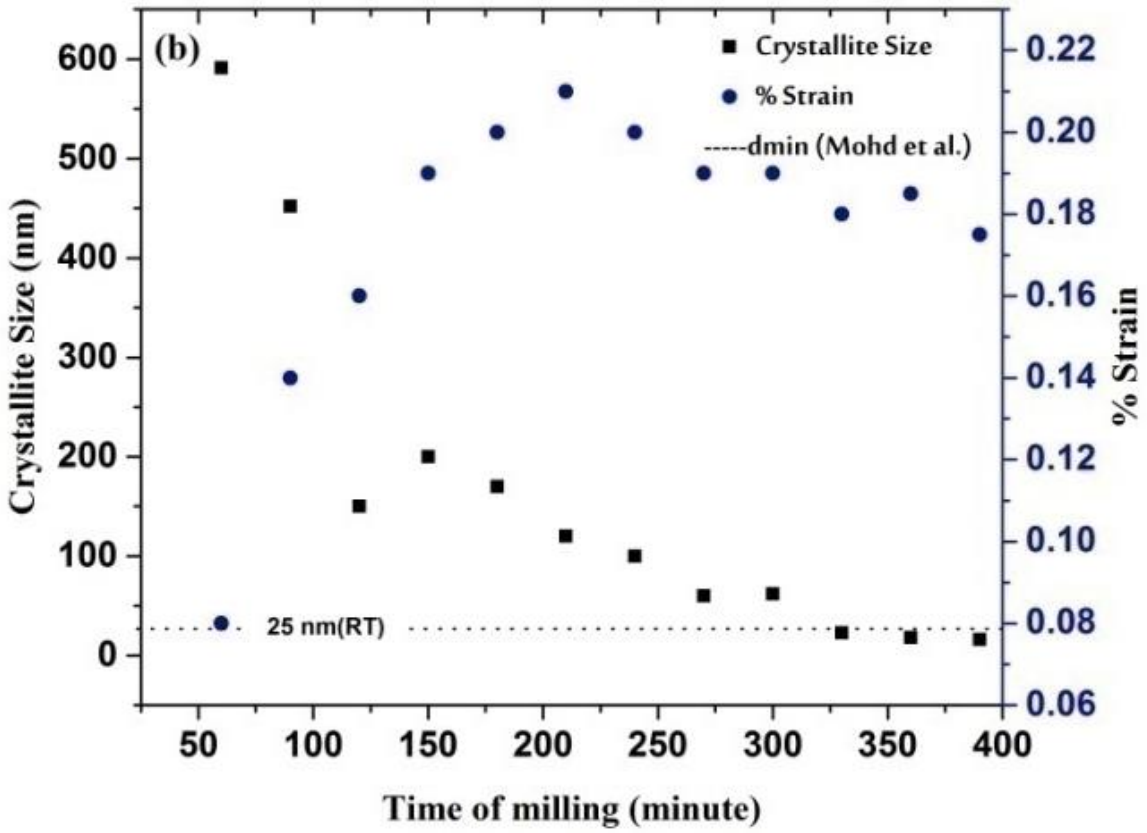

Figure 1: (a) X-ray diffraction pattern of Al cryomilled powder with different time of milling and; inset shows the broadening of (200) peak **(b)** crystallite size and strain variation of Al nanoparticles with time of milling.

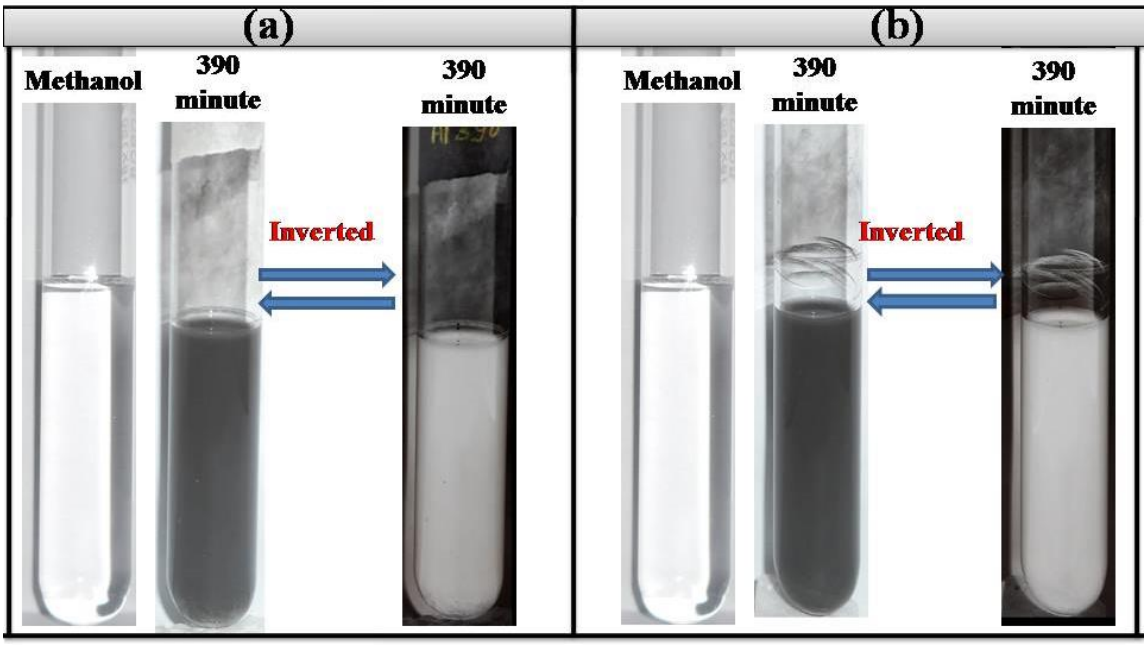

Figure 2: Cryomilled Al powder disperses in ultra high pure methanol (time of milling mentioned over test tube): **(a)** Just after preparation Al NPs and **(b)** after 10 days of dispersion.

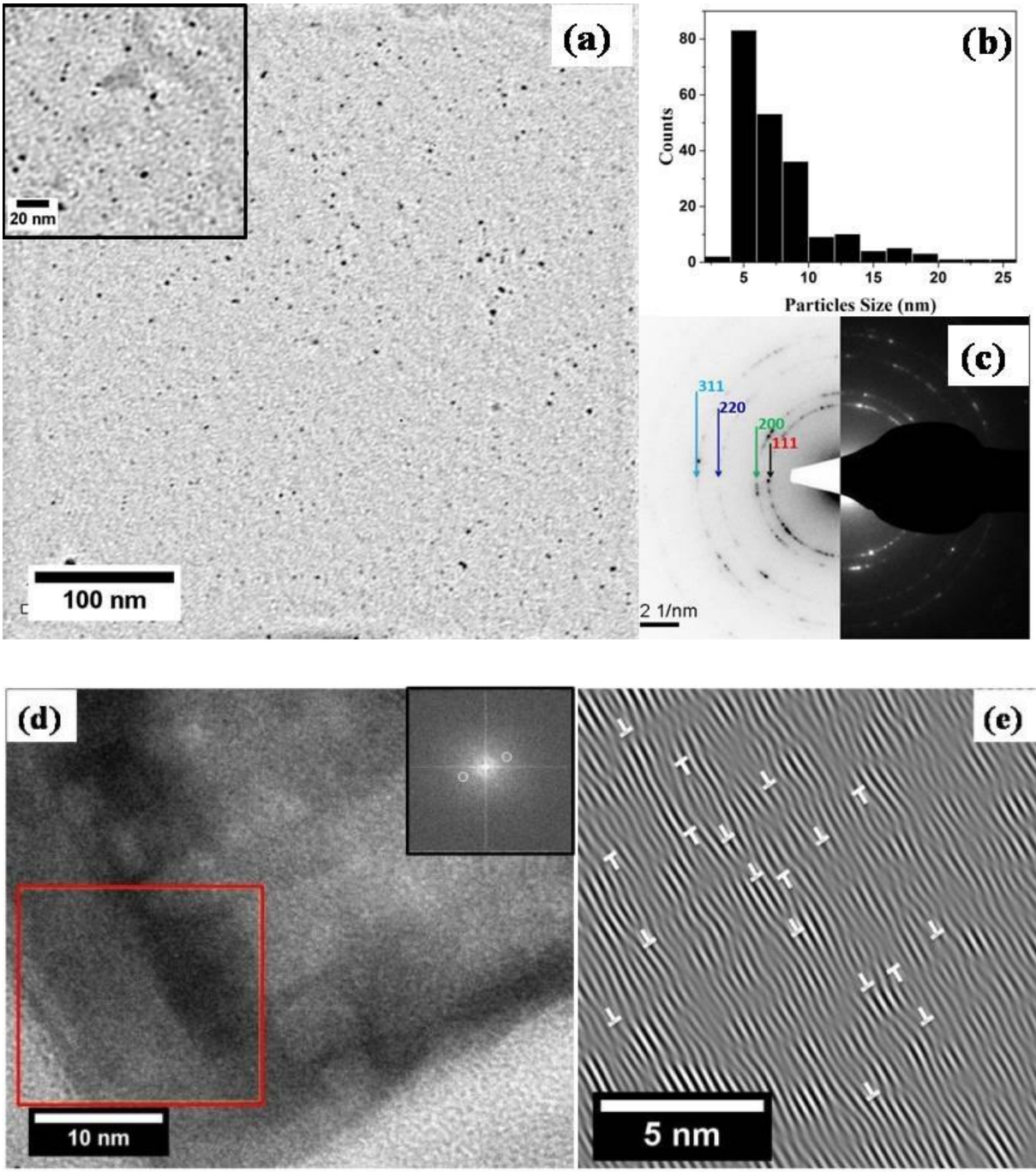

Figure 3: TEM images: **(a)** bright field TEM image of aluminium nanoparticles; **(b)** histogram showing distribution of nanoparticles; **(c)** correspondence diffraction pattern; **(d)** high resolution image of bigger particles; inset shows FFT of selected region **(e)** FFT filtered (masked) image showing edge dislocations.

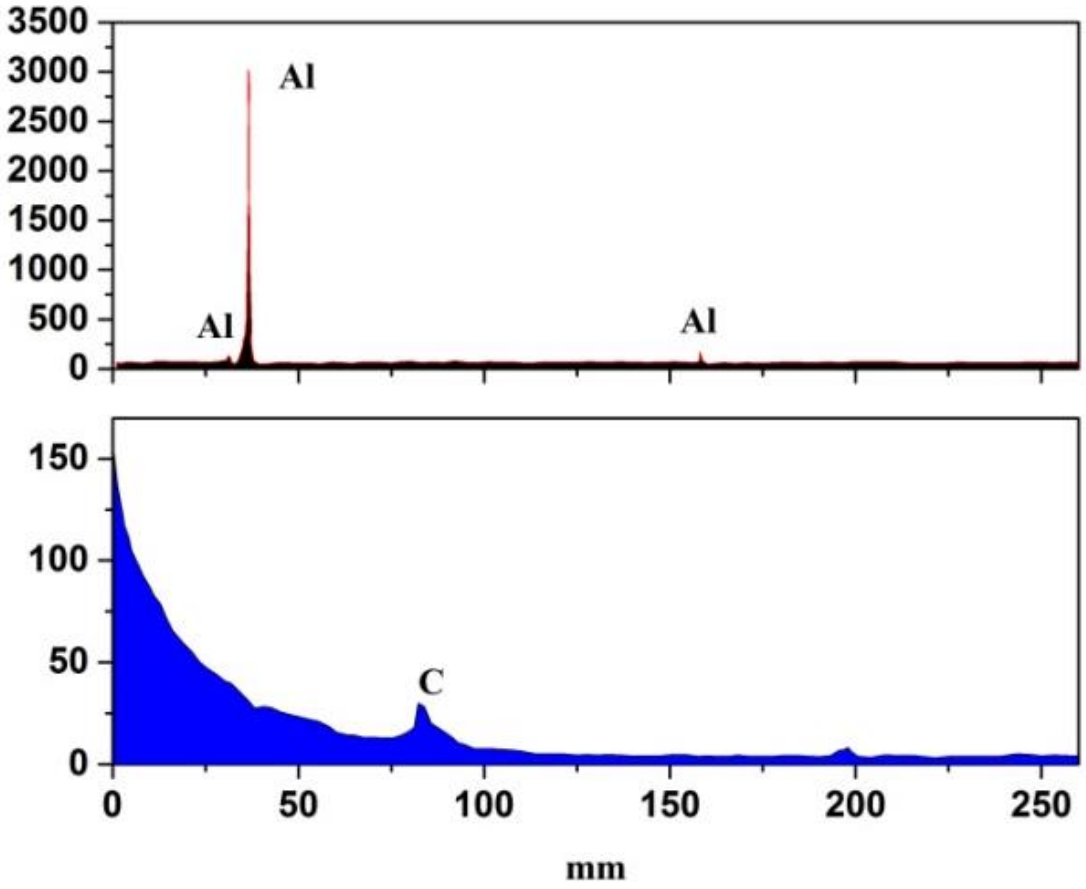

Figure 4: EPMA spectra (WDS) of powder cryomilled for 390 minute (Carbon from LDE crystal, Al from TAP crystal).

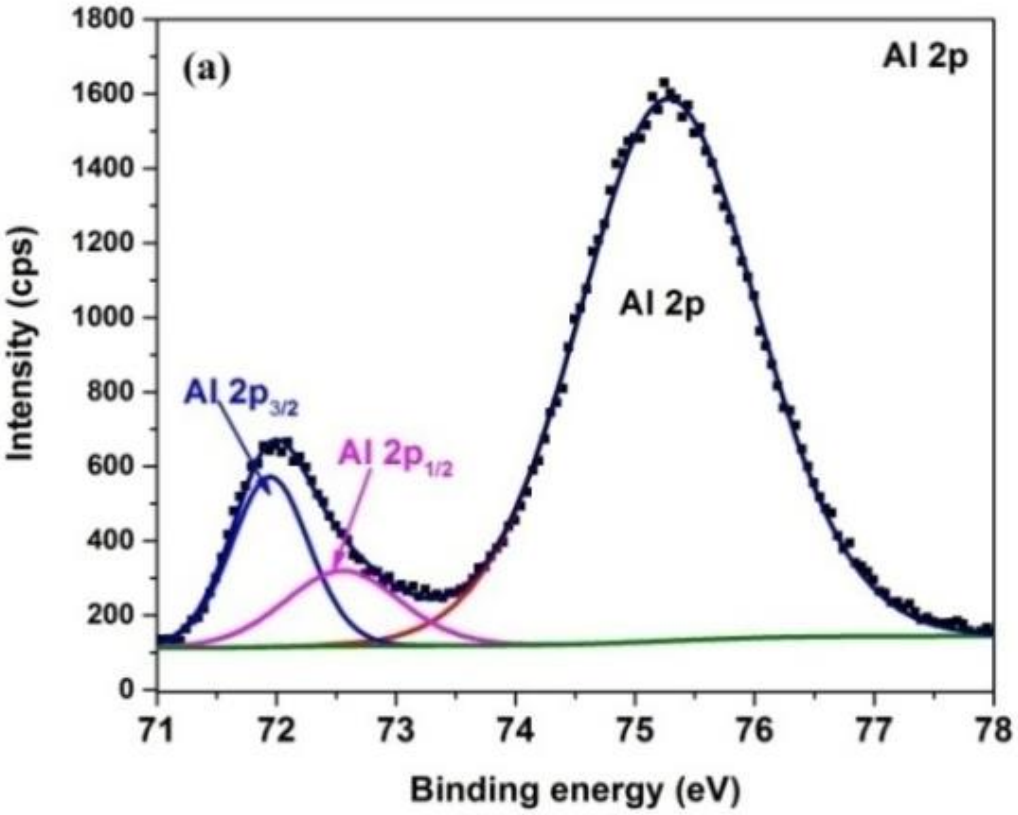
(a)
Al 2p
Al 2p
Al 2p3/2
Al 2p1/2
Intensity (cps)
Binding energy (eV)
1800
1600
1400
1200
1000
800
600
400
200
0
71
72
73
74
75
76
77
78

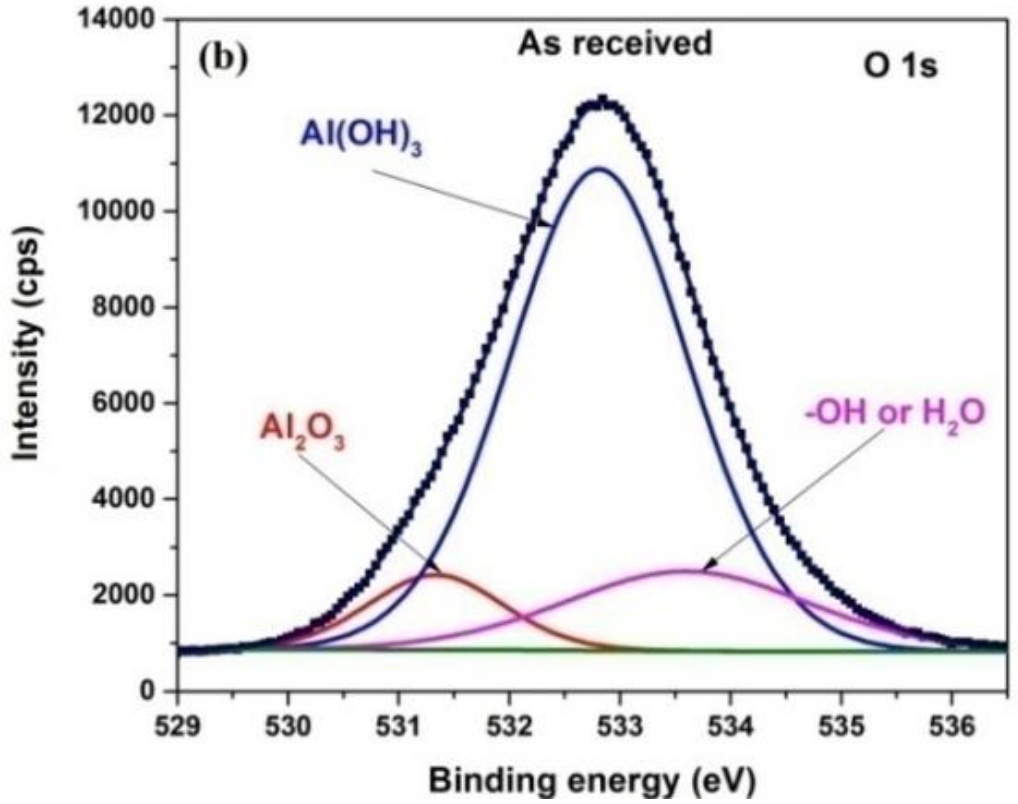
(b)
As received
O 1s
Al(OH)3
Al2O3
-OH or H2O
Intensity (cps)
Binding energy (eV)
14000
12000
10000
8000
6000
4000
2000
0
529
530
531
532
533
534
535
536

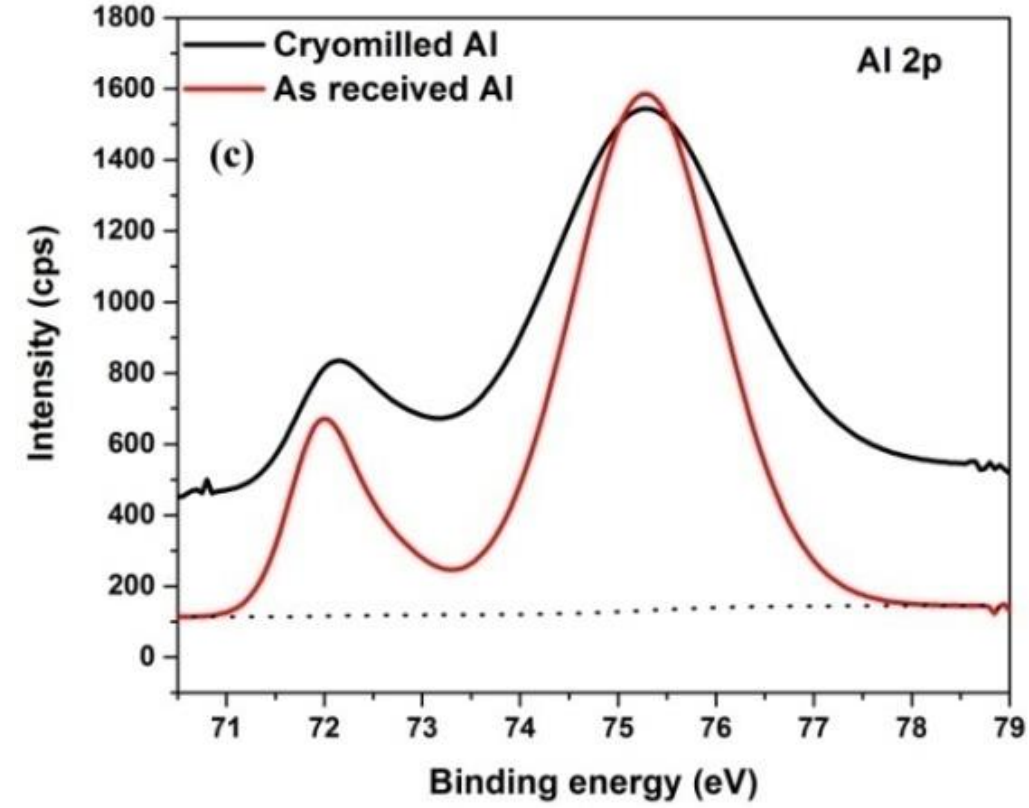
Cryomilled Al
As received Al
Al 2p
(c)
Intensity (cps)
Binding energy (eV)
1800
1600
1400
1200
1000
800
600
400
200
0
71
72
73
74
75
76
77
78
79

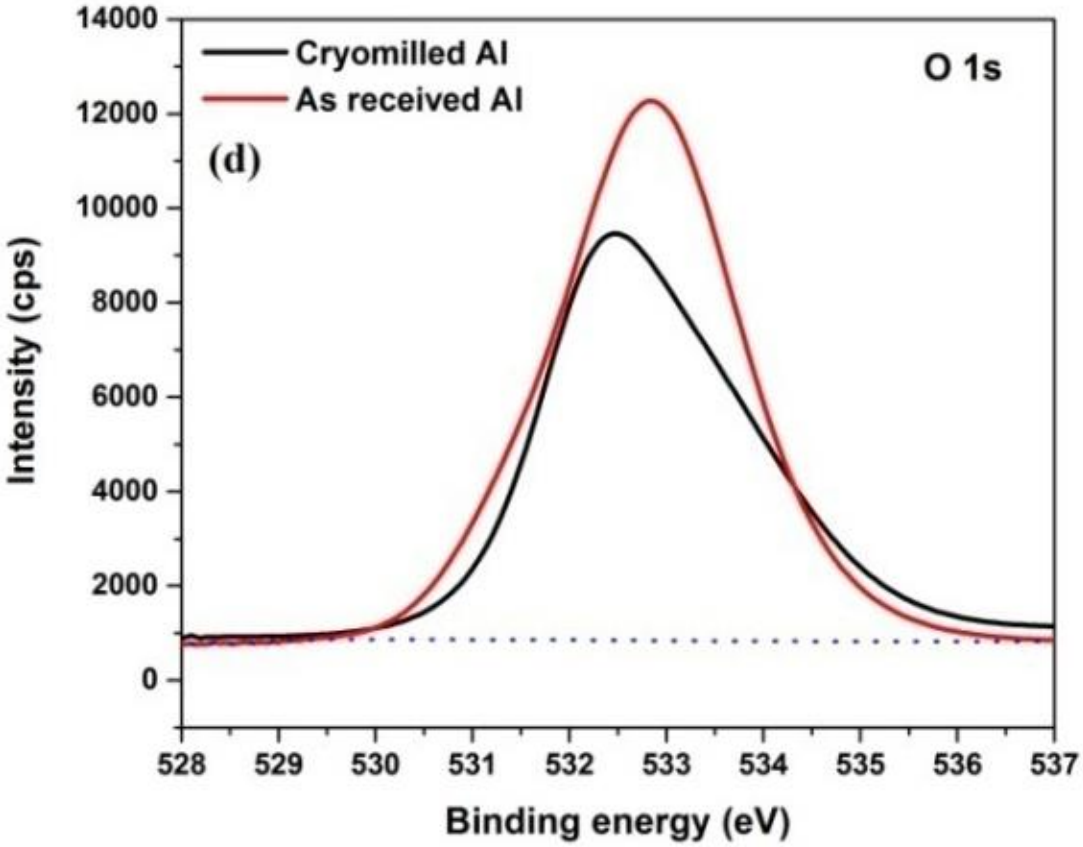
Cryomilled Al
As received Al
O 1s
(d)
Intensity (cps)
Binding energy (eV)
14000
12000
10000
8000
6000
4000
2000
0
528
529
530
531
532
533
534
535
536
537

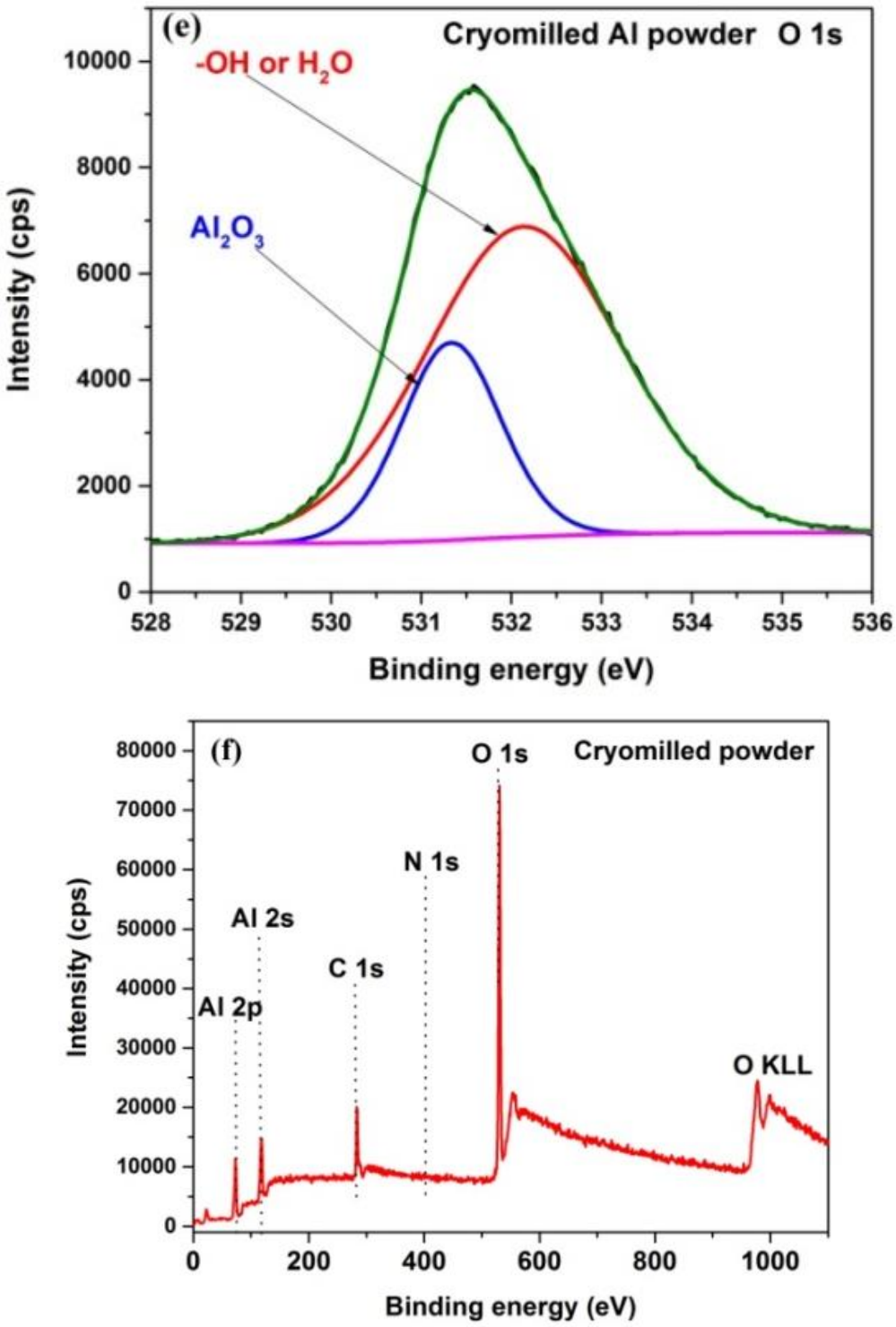

Figure 5: As received aluminium powder XPS spectra **(a)** Al 2p **(b)** O 1s **(c)** Al 2p **(d)** O1s **(e)** deconvolution of cryomilled Al O 1s peak **(f)** survey spectra of cryomilled Al nanopowder.

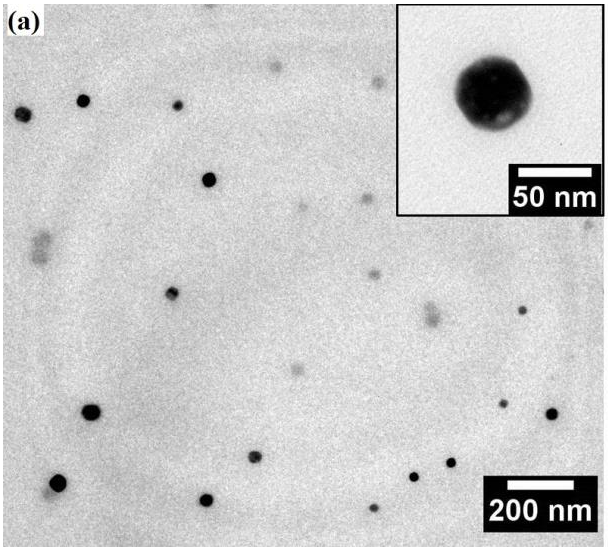
(a)
50 nm
200 nm

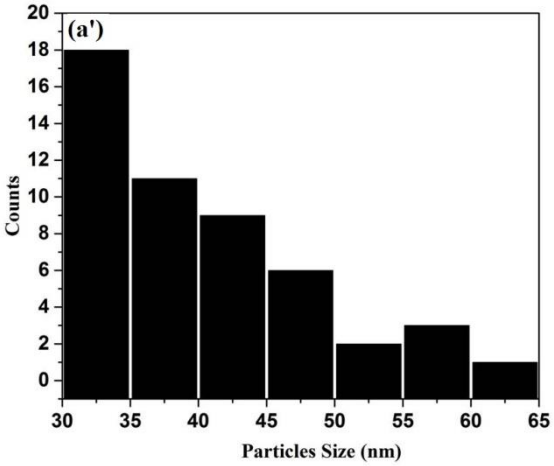
(a')
Counts
Particles Size (nm)

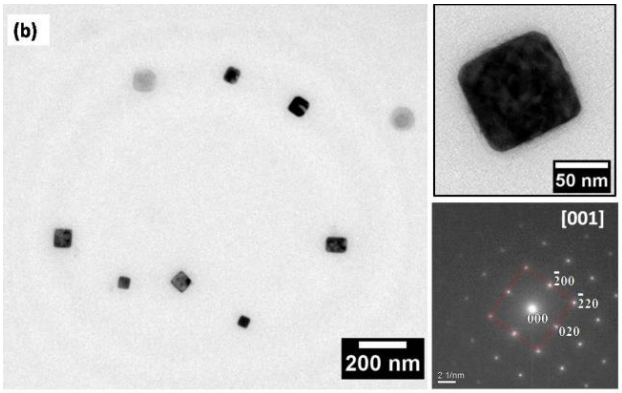
(b)
50 nm
[001]
200
220
000
020
200 nm

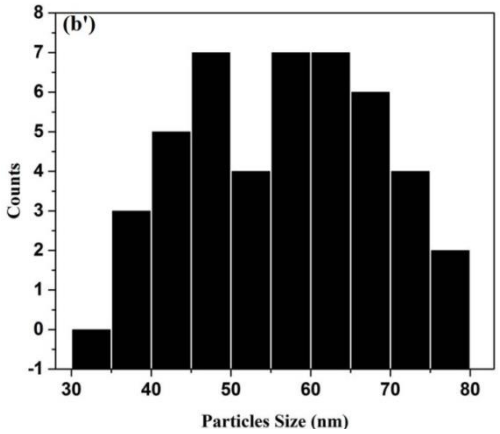
(b')
Counts
Particles Size (nm)

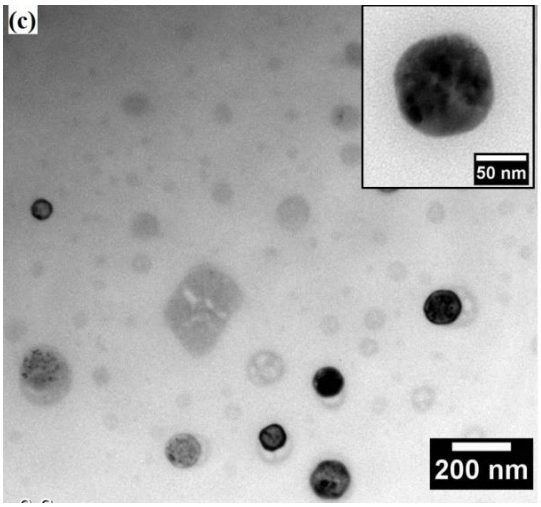
(c)
50 nm
200 nm

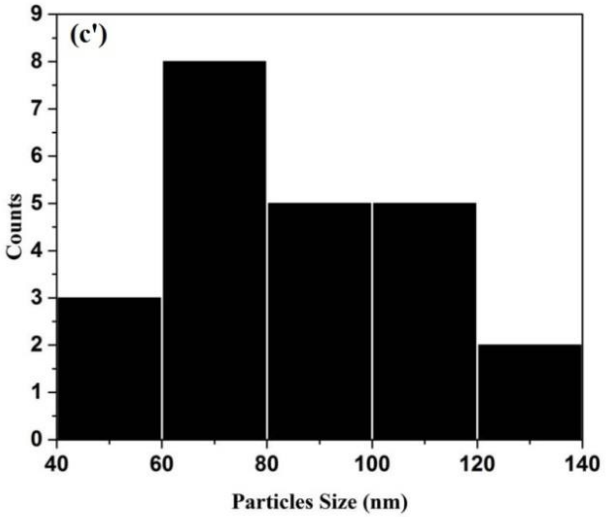
(c')
Counts
Particles Size (nm)

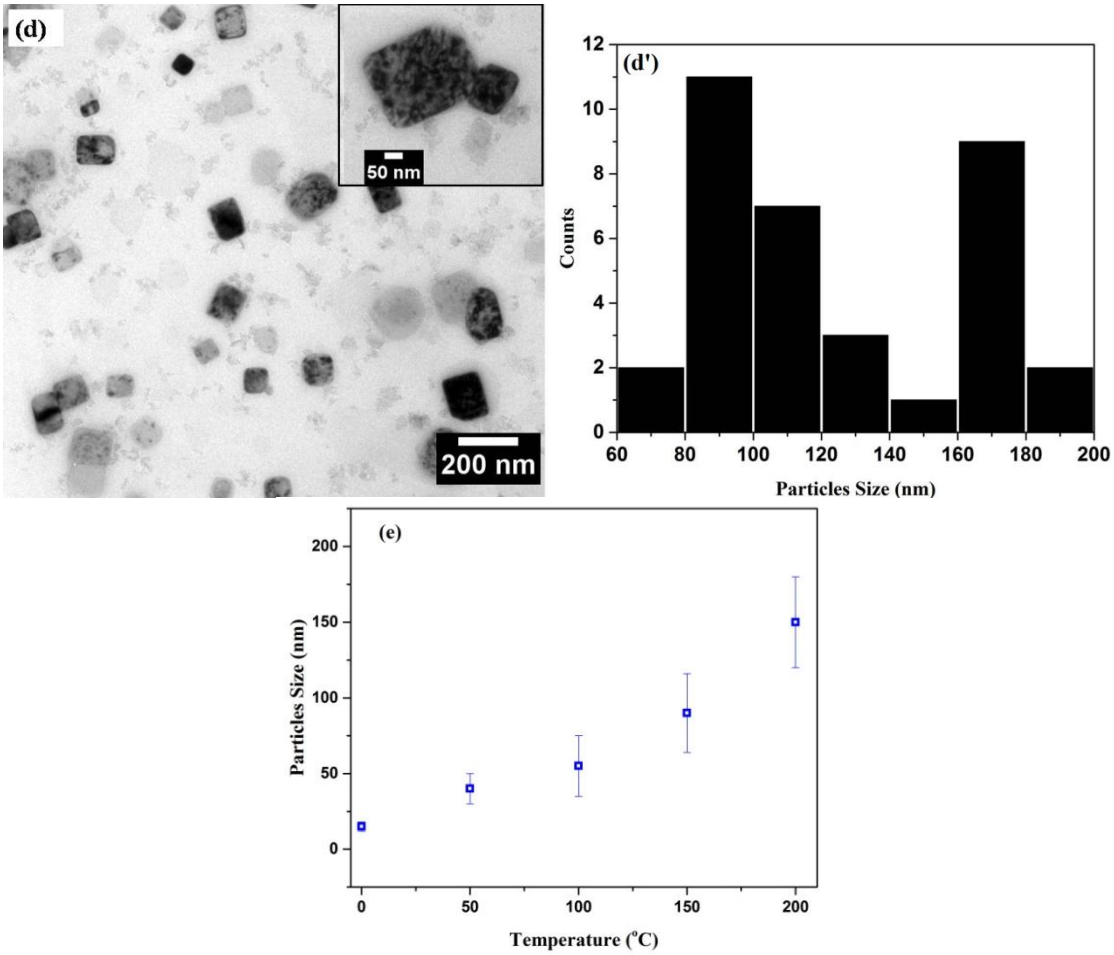

Figure 6: Transmission electron Microscope image after heat treatment with correspond size distribution: **(a)** at 323K (50 ^{o}C) for 2h ; **(b)** at 373K (100 ^{o}C) for 2h with inset showing SAD pattern from nanoparticle; (c) at 323K (150 ^{o}C) for 2h; (d) at 473K (200 ^{o}C) for 2h, lower inset in each figure showing corresponding particles size distribution; **(e)** coarsening of nanoparticles with temperature.

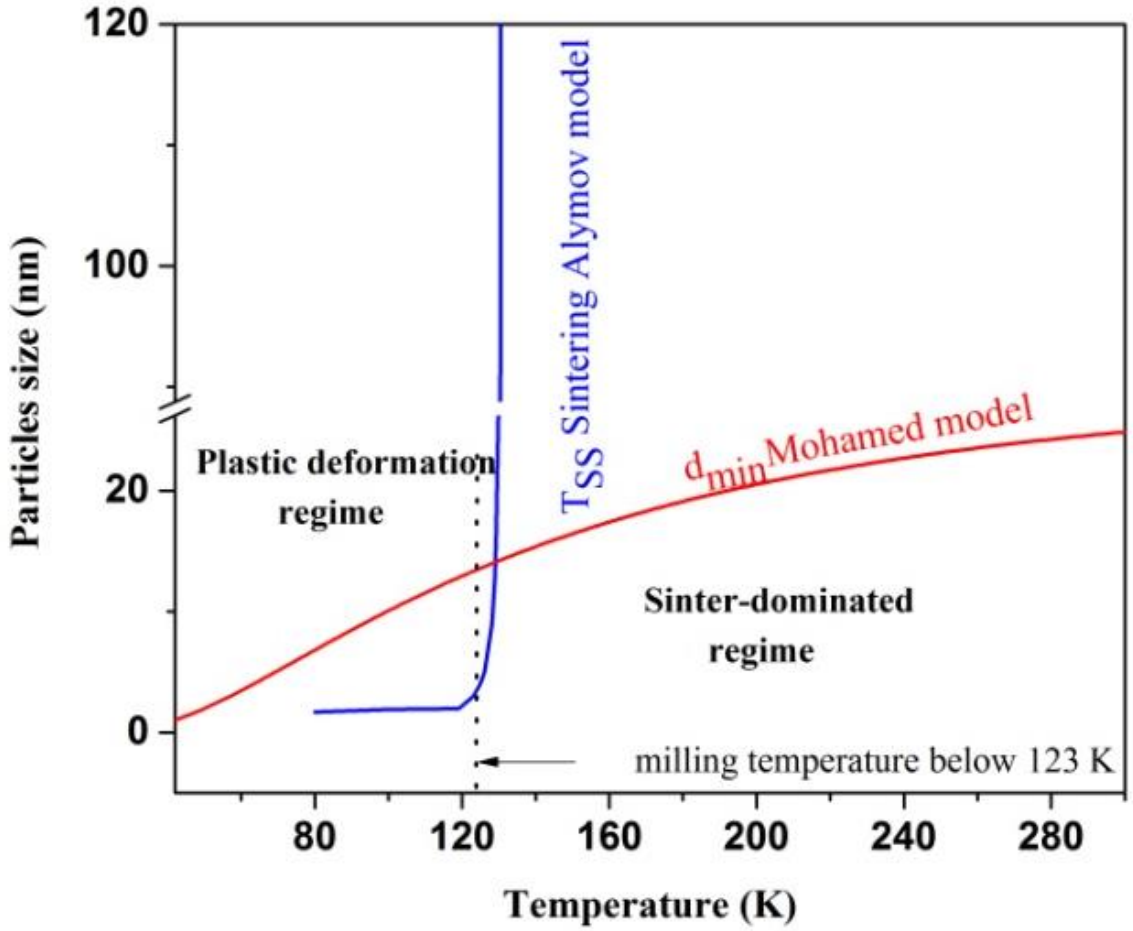

Figure 7: Crystallite size predicted by the model of Mohamed [33] (milling) and Alymov et. al.[34] (sintering) showing distinct regimes.

TOC

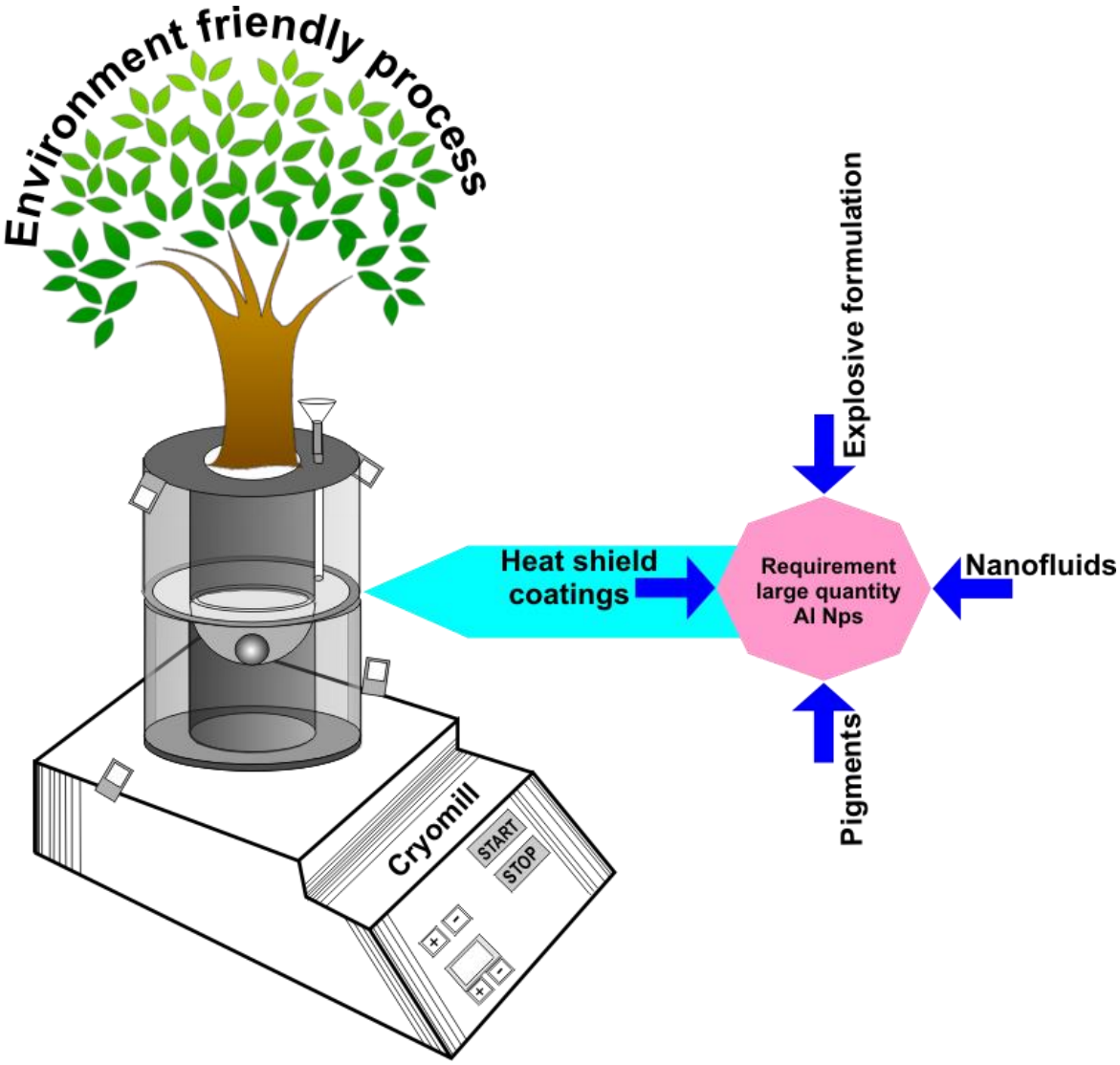
Environment friendly process
Explosive formulation
Heat shield coatings
Requirement large quantity Al Nps
Nanofluids
Pigments
Cryomill
START
STOP